NUKLEONIKA 2025;70(3):79–85
doi: 10.2478/nuka-2025-0008

ORIGINAL PAPER

sciendo

Dose enhancement effects of different-sized nanoparticles on tumors and surrounding tissues using Geant4 track structure simulation

Taylan Tuğrul

Abstract. Free radicals, which are the most important contributors to cell death in radiotherapy, appear to increase in the presence of nanoparticles. The nanoparticles can be localized within tumor tissues, providing enhanced protection to normal tissues during radiation therapy while achieving significant dose enhancement within tumors. In our study, the dose effects of different sizes of spherical gold nanoparticles were analyzed in the tumor environment and surrounding tissues under photon radiation at various energies with the track structure code using the TOPAS interface. The nano-lattice method was used to create an environment similar to the diffusion-based distribution of nanoparticles in the medium. The Geant4-DNA code was utilized for simulations conducted in this study. Although the interaction cross-section is lower at MeV photon energy levels, the results still indicate an increase in dose due to the presence of nanoparticles (NPs) in the medium. As the size of gold nanoparticles increases, the spread in dose enhancements becomes more apparent. The lowest average dose enhancement factor (DEF) values at lateral points were observed for 28.4 nm NPs at MeV photon energy. In this study, the contribution of gold nanoparticles to dose enhancement was investigated using the Monte Carlo track structure algorithm. Additionally, the potential dose variations in the surrounding tissue resulting from the introduction of gold nanoparticles were analyzed. Even though an increase in DEF values was observed at MeV energy levels, these values might vary with a better understanding of biological effects such as cell cycle disruption, oxidative stress, and impaired DNA repair. This study offers valuable insights into nanoparticle-assisted radiation applications, including optimal nanoparticle size and applicable energy levels. By enhancing our understanding of the effects on tissues beyond the tumor and within the surrounding environment, it aims to provide critical information for researchers in the field and make a meaningful contribution to the literature.

Keywords: Geant4 • Nanoparticle • TOPAS • Track structure

Introduction

Radiotherapy plays a crucial role in the effective application of cancer treatments [1]. Today, various methods are being explored to enhance the efficacy of radiotherapy while reducing its side effects. These include efforts to reduce the radiation resistance of tumor tissues and increase their radiosensitization, enhance the radioprotection of healthy tissues, and better confine the delivered dose to the tumor volume [2, 3].

The effectiveness of radiation therapies is typically evaluated by measuring the extent of DNA damage. However, damage to mitochondria can also lead to cell death. In other words, the disruption of membrane potential may induce apoptosis [2, 4–7]. Studies have shown that approximately 70% of DNA damage is caused by free radicals [3, 8–10]. In addition to damage caused by free radi-

T. Tuğrul
Department of Radiation Oncology
Faculty of Medicine
Van Yüzüncü Yıl University
Van, Turkey
E-mail: taylantugrul@gmail.com

Received: 10 March 2025
Accepted: 4 June 2025

cals, secondary electrons generated after radiation interacts with the medium can also contribute to DNA strand breaks [11].

The free radicals that contribute most significantly to cell death in radiotherapy show an increase in the presence of nanoparticles (NPs), making NPs a source of radiosensitization [12, 13]. Radiation excites the electrons of NPs in the medium, causing scattering. These excited electrons initiate the Auger process, leading to the emission of Auger electrons. Auger electrons typically have energies below 5 keV, and they ionize water molecules in the medium, contributing to the production of free radicals. Studies have also shown that Auger electrons are effective in directly damaging DNA [2, 14, 15]. Additionally, secondary electrons emitted by NPs interact with other NPs, contributing to the formation of more Auger electrons, which, when absorbed by the medium, increase free radical production [4, 12, 16]. Porcel *et al*. suggested that NPs could destabilize water molecules in the medium, facilitating their dissociation [12]. The properties of NPs, such as shape, size, concentration, chemical composition and distribution, have been shown to influence their radiosensitization effect [17, 18].

The permeability and retention effects of NPs allow for accumulation in tumors, enhancing contrast, enabling tumor-specific chemo-radiotherapy (CT-RT), and increasing the local radiation dose [19]. Tumor cells have larger intercellular gaps compared to normal tissues and exhibit richer vascularity. Additionally, structural deficiencies in the lymphatic drainage of tumor tissues result in the prolonged retention of macromolecules. This is why the terms "enhanced permeability and retention (EPR)" are used for tumor tissues. As a result, the permeability and uptake of NPs are higher in tumor cells [20–23]. Another study indicated that the elevated glutathione levels in tumor cells facilitate the accumulation of high atomic number NPs. As a result, NPs can be localized within tumor tissues, providing enhanced protection to normal tissues during radiation therapy while achieving significant dose enhancement within tumors [24].

The dose increase observed in the tumor region with the addition of NPs is attributed to the enhancement of the photoelectric effect cross-section [1, 25, 26]. The photoelectric cross-section is proportional to the atomic number of the interacting medium. In the presence of high atomic number NPs, photoelectron production is significantly higher [15]. As the atomic number increases, the probability of absorption due to the photoelectric effect also rises. However, as photon energy increases, the photoelectric effect decreases. Consequently, the interaction of high atomic number NPs with low-energy photons results in a higher dose enhancement in the target medium.

Gold nanoparticles (NP-G) possess properties that make them advantageous for targeting cancer cells [3, 16, 27–31]. NP-Gs are typically clustered particles ranging in size from 1 nm to 150 nm. Their tunable size, shape, surface properties, and chemical structure are among their most critical features [19, 32, 33]. NPs amplify radiation effects through physical, chemical, and biological interactions in the medium. In the physical phase, secondary electrons, Auger electrons, and free radicals are effective in inducing cell death. The surface of NP-Gs catalyzes free radical formation, and low-energy electrons sensitize DNA to radiation, which is part of the chemical aspect. In the biological phase, NP-Gs enhance radiation effects by inducing oxidative stress, disrupting the cell cycle, and impairing DNA repair mechanisms [19]. Monte Carlo (MC) simulations are widely utilized in nanoparticle-assisted radiation applications. MC simulations have become a vital tool in these studies, employing mathematical algorithms to simulate radiation transport in the medium. They can accurately predict dose distributions in NP-assisted biological systems by modeling at a subatomic level [26, 34, 35]. Moreover, MC simulations are instrumental in understanding the physical mechanisms responsible for dose enhancement in NP-assisted radiation applications.

Track structure (TS) and condensed history (CH) are two distinct algorithms used in MC simulations to model the interaction of radiation with matter. Both algorithms are widely utilized for simulating radiation interactions, differing primarily in terms of precision and computational time. The TS algorithm tracks all interactions in detail, modeling each interaction individually. Particles interacting with matter can be tracked at nanometer or even atomic scales. The TS algorithm provides high accuracy for studies conducted at nanometer scales, making it particularly important for calculations at the cellular level. However, because each interaction is modeled, it requires significant computational power and time, rendering it impractical for macroscopic simulations. In contrast, the CH algorithm summarizes multiple small-scale interactions into a single step. Its accuracy is limited for simulations at nanometer scales and is unsuitable for modeling particle behavior in microscopic environments or interactions with specific targets like DNA. In Monte Carlo applications, when simulations at the nanoscale are required, TS simulations should be preferred [36–38].

Various TS codes, such as Geant4, RITRACKS, and KURBUC, are commonly used in nanoparticle studies [17, 37, 39]. Among them, Geant4-DNA, an extension of the Geant4 simulation toolkit, is a validated tool designed for modeling at the cellular level. It is tailored for accurate modeling at nanoscales, down to energies as low as eV, using the TS algorithm. TOPAS (Tool for Particle Simulation) is a software interface utilizing the Geant4 MC toolkit and is specifically designed for applications in radiation therapy, medical imaging, and radiobiology. It allows MC simulations of all types of ionizing radiation, including in complex geometries and at nanoscales [17, 40]. There is limited literature on the dose variations in surrounding tissues caused by nanoparticles added to tumor tissues. In our study, the dose effects of different sizes of spherical nanoparticles were analyzed in the tumor environment and surrounding tissues under photon radiation at various energies with the TS code using the TOPAS interface. The findings from the interac-

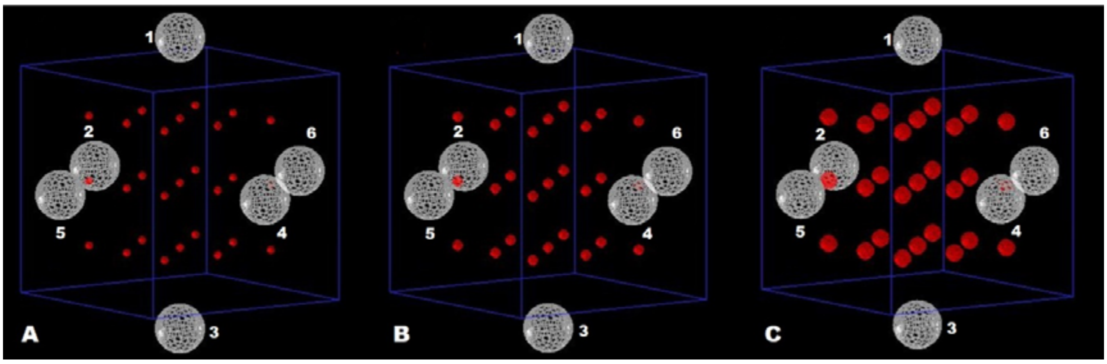

Fig. 1. Three different nanoparticles sizes in the Lattice Box: A – 20 nm, B – 28.4 nm, C – 50 nm.

tions of radiation with nanoparticles at nanoscales are critical for understanding the physical mechanisms and their effects on surrounding tissues. Additionally, this knowledge can guide researchers in designing more effective nanoparticles. This could contribute to advancing the use of nanoparticles in radiotherapy, highlighting their significant potential in improving cancer treatment methodologies.

Material and methods

Gold material was selected as the nanoparticle. The nano-lattice method was used to create an environment similar to the diffusion-based distribution of NPs in the medium. To realistically model the distribution of NPs within cells, a specific number of NPs were placed in nanoscale cubes [20]. In the nano-lattice method, a certain number of NPs selected for the study are placed homogeneously in an environment with a density similar to water, with equal distances between them. The use of the TS algorithm at nanoscales allows the modeling of low-energy electrons produced by NPs with high accuracy. Therefore, the Geant4-DNA code was utilized for simulations conducted in this study. This code can track and model electrons down to the excitation energy of water molecules [15].

Figure 1 shows the geometric arrangement of NPs. The NP-Gs were distributed homogeneously within a cube. NP-Gs with sizes of 20 nm, 28.4 nm, and 50 nm were placed inside a 700 × 700 × 700 nm^3 water cube. When we increase the NP size, since the Lattice Box volume and the number of NPs are constant, in fact the concentration is also increased. For NP sizes of 20 nm, 28.4 nm, and 50 nm, the NP-G concentrations in the medium were 6.33 mg/g, 17.9 mg/g, and 90.9 mg/g, respectively. The concentration was calculated by determining the ratio of the total mass of the nanoparticles to the mass of the surrounding medium. For this purpose, the volume and known density of each spherical nanoparticle were used to calculate the total particle mass. Subsequently, the mass of the cubic medium was obtained using its volume and density. These two values were then used to express the concentration in mg/g. The size of the radiation beam must be at least 10 times larger than the NP size to effectively track the secondary electrons produced by the NPs [15]. Otherwise, the dose enhancement factor (DEF) may vary significantly. The radiation field size was set to 1500 × 1500 nm^2. The distance from the source to the lattice surface is 1100 nm. Additionally, dose variations in surrounding tissues due to the presence of NP-Gs were analyzed. The dose measurement points examined are shown as 1, 2, 3, 4, 5, and 6 in Fig. 1. Point 5 is positioned in front of the phantom along the beam direction, while point 6 is located behind the phantom along the beam's exit direction. Points 1, 2, 3, and 4 are positioned laterally at equal distances around the phantom.

In our study, simulations were modeled using the TOPAS interface for the geometric structure in Fig. 1 at photon energies of 80 keV, 250 keV, and 3 MeV. The latest version of Geant4, Geant4-DNA, can model not only physical interactions but also chemical processes such as free radical production, diffusion, and DNA strand breaks [15]. Accurate definition of the physics package is crucial for MC simulations, especially at low energies and small scales. Since our simulations were conducted at the nanoscale to track the dose in cellular dimensions and radiation interactions accurately, the g4em-dna_opt7 module of the Geant4 code was employed. To minimize uncertainties, the number of histories was set to 1×10^9. In the physics settings of the MC simulations, fluorescent radiation, Auger effect, particle-induced X-ray emission (PIXE), and Auger cascade interactions were activated. Since the study requires a large number of simulations, computation times can be very high. Powerful workstations are needed to minimize computation times and uncertainty. The workstation used in this study was supported by Research Fund of the Van Yüzüncü Yıl University project no. 11418. The materials representing normal tissue in the simulation were composed of 76.2% oxygen, 2.6% nitrogen, 11.1% carbon, and 10.1% hydrogen, as defined by the International Commission on Radiation Units and Measurements (ICRU) [41]. The DEF is used to evaluate the effectiveness of NPs in radiotherapy. DEF is defined as the ratio of the dose measured with NPs to the dose measured without NPs. This value can vary depending on the location, concentration, and properties of the NPs [2]. In simulations conducted with and without NPs, beam geometry and physics parameters were adjusted identically across all MC codes.

Results

For NP-G sizes of 20 nm, 28.4 nm, and 50 nm within the lattice, the DEF values for 80 keV photon energy were found to be 1.0615, 1.2222, and 2.2874, respectively. For 250 keV photon energy, these values were measured as 1.0843, 1.1493, and 2.0350, respectively. For 3 MeV photon energy, the DEF values were determined to be 0.9923, 1.0856, and 1.4724, respectively. The results clearly show that as the NP-G size increases, the DEF values also increase. Although the interaction cross-section is lower at MeV photon energy levels, the results still indicate an increase in dose due to the presence of NPs in the medium. Studies have shown that the dose increase observed at these energy levels is due to the interaction of NPs with secondary radiation produced by the ionization of the water environment [2, 27]. At MeV energy levels, while the cross-sections for Compton scattering and pair production increase slightly, the DEF remains low due to the reduced photoelectric effect. Electrons generated at these levels do not significantly contribute to the dose, so substantial dose enhancement is not expected in this range. Additionally, a study by Robar *et al*. demonstrated that the removal of the flattening filter in a linear accelerator device could enhance the effect of the low-energy component in the spectrum on dose enhancement [42]. The DEF values of nanoparticles of different sizes in the lattice after applying different radiation energies are shown in Fig. 2. As the size of gold nanoparticles increases, the spread in dose enhancements becomes more apparent, as observed in the Fig. 2.

When we examine the DEF values at the dose measurement point 5 in front of the phantom in the direction of the incident beam: for 80 keV photon energy, the DEF values for 20 nm, 28.4 nm, and 50 nm NPs were measured as 1.0453, 1.0421, and 1.3354, respectively. For 250 keV photon energy, these values were found to be 0.9286, 0.9585, and 1.0487, respectively. For 3 MeV photon energy, the DEF values at this point were 1.0174, 1.0810, and 1.0112, respectively. While the dose values at MeV photon energy levels varied when NPs were present, the results clearly show that for 80 keV photon energy with 50 nm NPs, the dose was significantly higher. The DEF values obtained at measurement point 5 are shown in Fig. 3.

DEF values of the dose measurement point 6 behind the phantom at the exit point of the beam direction: for 80 keV photon energy, the DEF values for 20 nm, 28.4 nm, and 50 nm NPs were 0.8576, 0.9068, and 0.9843, respectively. For 250 keV photon energy, these values were measured as 0.9835, 1.0054, and 1.0749. For 3 MeV photon energy, the DEF values at point 6 were 1.0628, 1.0368, and 1.5236, respectively. The simulation results indicate that for all NP sizes, the dose at the rear of the phantom increased with energy. The lowest DEF was observed at 80 keV with 20 nm NPs, while the highest was at 3 MeV with 50 nm NPs. The higher DEF at MeV photon energy levels is attributed to the deeper penetration of photons, leading to increased ionizations and more interactions compared to keV photon levels. The DEF values obtained at measurement point 6 are shown in Fig. 4.

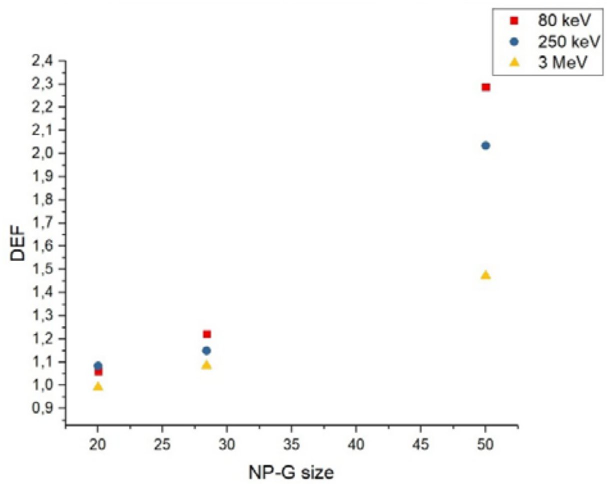

Fig. 2. DEF values of nanoparticles of different sizes in the lattice under different energies.

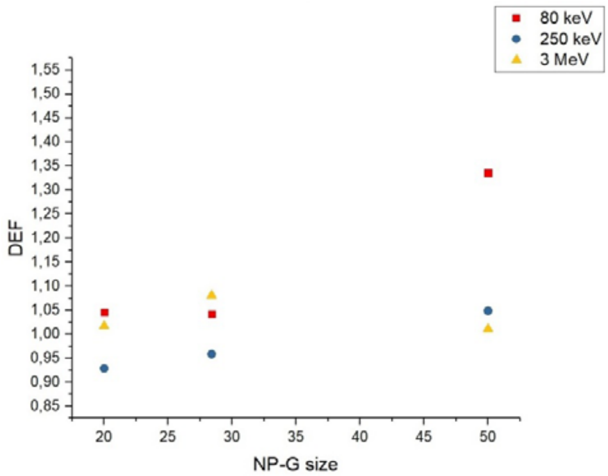

Fig. 3. DEF values obtained at measurement point 5 as a result of adding nanoparticles of different sizes to the medium.

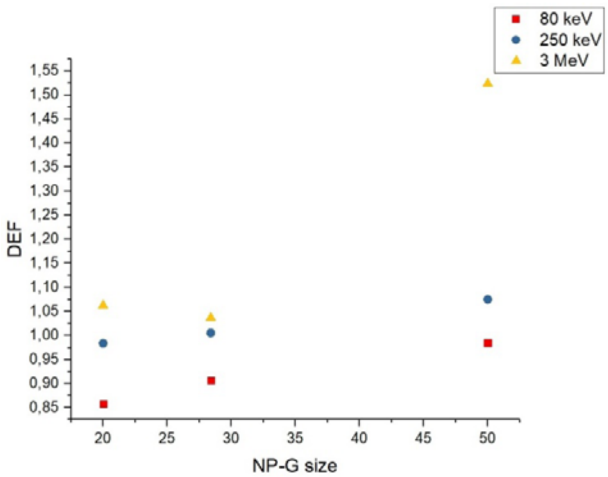

Fig. 4. DEF values obtained at measurement point 6 as a result of adding nanoparticles of different sizes to the medium.

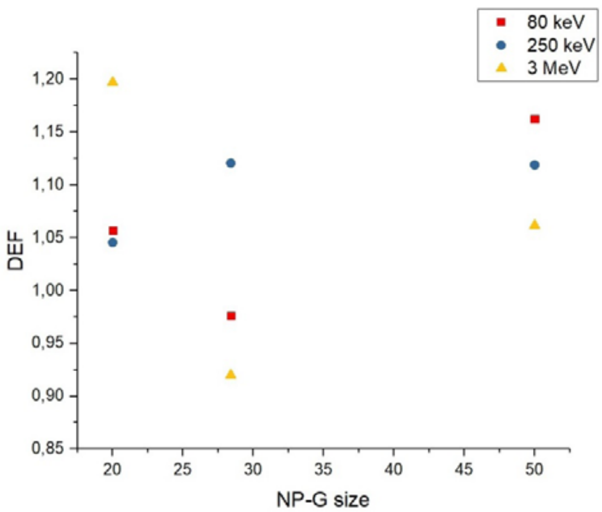

Fig. 5. The average DEF values obtained at lateral measurement points as a result of adding nanoparticles of different sizes to the medium.

The average DEF values for lateral points were also calculated from the simulation results. At 80 keV photon energy, the average DEF values for 20 nm, 28.4 nm, and 50 nm NPs were 1.0569, 0.9764, and 1.1622, respectively. At 250 keV photon energy, the average DEF values were 1.0453, 1.1205, and 1.1188, respectively. For 3 MeV photon energy, the average DEF values were 1.1969, 0.9199, and 1.0615, respectively. For 50 nm NPs, a decrease in the average DEF at lateral points was observed as the energy increased. For 20 nm NPs, the highest DEF values were measured at MeV energy levels. The lowest average DEF values at lateral points were observed for 28.4 nm NPs at MeV photon energy. The average DEF values obtained at lateral measurement points are shown in Fig. 5.

Discussion and conclusion

In this study, the contribution of NP-G to dose enhancement was investigated using the Monte Carlo TS algorithm. Additionally, the potential dose variations in the surrounding tissue resulting from the introduction of NP-G were analyzed. The study also demonstrated the significant role of nanoparticle size in dose enhancement values. The number of atoms present in the tissue medium is lower than the number of atoms in the added nanoparticles. This excess in atomic number enhances photoelectric effects and increases Compton interactions as energy rises, leading to secondary particle production and an accumulation of higher doses in the medium. Although larger nanoparticles were shown to provide greater dose enhancement, concluding that they are the best choice without considering other factors may not be accurate. Issues such as the biological uptake of nanoparticles by cells, toxicity related to size, and other biophysical effects need further investigation. The amount of dose reaching the points outside the lattice may be higher in the absence of NPs. Nanoparticles located close to the lattice surface absorb more dose, leading to a decrease in the number of electrons reaching the surface boundary. This effect is more pronounced at low photon energies. The reason why the DEF value is less than 1 at low energies can be attributed to this reason. As the energy and size increase, the DEF value will be greater than 1 because the number of secondary particles will increase and the NP boundary will approach the lattice surface. Even though an increase in DEF values was observed at MeV energy levels, these values might vary with a better understanding of biological effects such as cell cycle disruption, oxidative stress, and impaired DNA repair. Once in the body, NPs can also elicit an immune response. Factors such as cell cycle disruption, oxidative stress, impaired DNA repair, inflammatory response and interference with cell signaling pathways can disrupt gene expression and promote cell death. This highlights the potential for developing new radiation methodologies, enabling more effective treatments. Interdisciplinary studies are essential to evaluate these factors in clinical applications. The underlying mechanisms causing dose enhancement following nanoparticle addition remain to be fully elucidated. Several considerations need to be addressed for selecting appropriate nanoparticles, including the material type, size, shape, surface coatings, clearance from the liver, potential toxicity, cellular uptake, and biological responses. Nanotechnology holds the potential to make significant contributions to the field of radiotherapy. MC simulations evaluating the effects of NPs in radiotherapy, the physical interaction phase is the most decisive component. This stage includes phenomena such as the photoelectric effect, Compton scattering, and Auger electron production, which directly determine the increase in dose within the medium. Particularly when high atomic number NPs interact with low-energy X-rays, photoelectric events dominate and lead to significant dose enhancement. In contrast, the chemical and biological phases (e.g., free radical formation and DNA damage) are modeled subsequently or indirectly, and are often excluded due to the high computational cost of simulating them in full detail. Although toolkits like Geant4-DNA can model these processes, most studies remain limited to the physical phase alone. This implies that MC simulations primarily estimate the physical dose enhancement, rather than the full biological impact. However, literature has reported a strong correlation between increased physical dose and enhanced biological effect, suggesting that focusing on the physical phase can still offer meaningful predictions of treatment effectiveness [43]. Nonetheless, for a more comprehensive evaluation, it is recommended that the chemical and biological processes also be taken into account alongside physical interactions. This study offers valuable insights into nanoparticle-assisted radiation applications, including optimal nanoparticle size and applicable energy levels. By enhancing our understanding of the effects on tissues beyond the tumor and within the surrounding environment, it aims to provide critical information for researchers in the field and make a meaningful contribution to the literature. The findings of this study could also serve to accelerate experimental research and facilitate future advancements.

Conflict-of-interest statement. The author has no relevant financial or non-financial interests to disclose. The author has no competing interests to declare that are relevant to the content of this article.

ORCID

T. Tuğrul https://orcid.org/0000-0002-0557-1334

References

1. Kakade, N. R., & Sharma, S. D. (2015). Dose enhancement in gold nanoparticle-aided radiotherapy for the therapeutic photon beams using Monte Carlo technique. *J. Cancer Res. Ther.*, *11*, 94–97.
2. Haume, K., Rosa, S., Grellet, S., Smialek, M. A., Butterworth, K. T., Solov'yov, A. V., Prise, K. M., Golding, J., & Mason, N. J. (2016). Gold nanoparticles for cancer radiotherapy: a review. *Cancer Nano.*, *7*, 8.
3. Kwatra, D., Venugopal, A., & Anant, S. (2013). Nanoparticles in radiation therapy: a summary of various approaches to enhance radiosensitization in cancer. *Transl. Cancer Res.*, *2*(4), 330–342.
4. Kobayashi, K., Usami, N., Porcel, E., Lacombe, S., & Le Sech, C. (2010). Enhancement of radiation effect by heavy elements. *Rev. Mutat. Res.*, *704*(1/3), 123–131.
5. Pan, Y., Leifert, A., Ruau, D., Neuss, S., Bornemann, J., Schmid, G., Brandau, W., Simon, U., & Jahnen Dechent, W. (2009). Gold nanoparticles of diameter 1.4 nm trigger necrosis by oxidative stress and mitochondrial damage. *Small*, *5*(18), 2067–2076.
6. Taggart, L. E., McMahon, S. J., Currell, F. J., Prise, K. M., & Butterworth, K. T. (2014). The role of mitochondrial function in gold nanoparticle mediated radiosensitisation. *Cancer Nanotechnol.*, *5*(1), 5.
7. Taggart, L. E., McMahon, S. J., Butterworth, K. T., Currell, F. J., Schettino, G., & Prise, K. M. (2016). Protein disulphide isomerase as a target for nanoparticle-mediated sensitisation of cancer cells to radiation. *Nanotechnology*, *27*(21), 215101.
8. Kavanagh, J. N., Redmond, K. M., Schettino, G., & Prise, K. M. (2013). DNA double strand break repair: a radiation perspective. *Antioxid. Redox Signal.*, *18*(18), 2458–2472.
9. Nikjoo, H., O'Neill, P., Wilson, W. E., & Goodhead, D. T. (2001). Computational approach for determining the spectrum of DNA damage induced by ionizing radiation. *Radiat. Res.*, *156*(5), 577–583.
10. Emfietzoglou, D., Cucinotta, F. A., & Nikjoo, H. (2005). A complete dielectric response model for liquid water: a solution of the Bethe ridge problem. *Radiat Res.*, *164*(2), 202–211.
11. Pan, X., Cloutier, P., Hunting, D., & Sanche, L. (2003). Dissociative electron attachment to DNA. *Phys. Rev. Lett.*, *90*, 208102.
12. Porcel, E., Liehn, S., Remita, H., Usami, N., Kobayashi, K., Furusawa, Y., Le Sech, C., & Lacombe, S. (2010). Platinum nanoparticles: a promising material for future cancer therapy? *Nanotechnology*, *21*, 085103.
13. Verkhovtsev, A. V., Korol, A. V., & Solov'yov, A. V. (2015). Electron production by sensitizing gold nanoparticles irradiated by fast ions. *J. Phys. Chem. C*, *119*(20), 11000–11013.
14. Butterworth, K. T., McMahon, S. J., Taggart, L. E., & Prise, K. M. (2013). Radiosensitization by gold nanoparticles: effective at megavoltage energies and potential role of oxidative stress. *Transl. Cancer Res.*, *2*(4), 269–279.
15. Moradi, F., Rezaee Enrahim Saraee, Kh., Abdul Sani, S. F., & Bradley, D. A. (2021). Metallic nanoparticle radiosensitization: The role of Monte Carlo simulations towards progress. *Radiat. Phys. Chem.*, *180*, 109294.
16. Hainfeld, J. F., Dilmanian, F. A., Slatkin, D. N., & Smilowitz, H. M. (2008). Radiotherapy enhancement with gold nanoparticles. *J. Pharm. Pharmacol.*, *60*(8), 977–985.
17. Taheri, A., Khandaker, M. U., Moradi, F., & Bradley, D. A. (2024). A simulation study on the radiosensitization properties of gold nanorods. *Phys. Med. Biol.*, *69*, 045029.
18. He, W., Ma, G., Shen, Q., & Tang, Z. (2022). Engineering gold nanostructures for cancer treatment: spherical nanoparticles, nanorods, and atomically precise nanoclusters. *Nanomaterials*, *12*, 1738.
19. Her, S., Jaffray, D. A., & Allen, C. (2017). Gold nanoparticles for applications in cancer radiotherapy: Mechanisms and recent advancements. *Adv. Drug Deliv. Rev.*, *109*, 84–101.
20. Çağlar, M., Eşitmez, D., & Cebe, M. S. (2024). The effect of dose enhancement in tumor with silver nanoparticles on surrounding healthy tissues: A Monte Carlo study. *Technology in Cancer Research & Treatment*, *23*, 1–8.
21. Wu, J. (2021). The enhanced permeability and retention (Epr) effect: The significance of the concept and methods to enhance its application. *J. Pers. Med.*, *11*(8), 771–779.
22. Matsumura, Y., & Maeda, H. (1986). A new concept for macromolecular therapeutics in cancer chemotherapy: Mechanism of tumoritropic accumulation of proteins and the antitumor agent smancs. *Cancer Res.*, *46*(8), 6387–6392.
23. Mesbahi, A. (2010). A review on gold nanoparticles radiosensitization effect in radiation therapy of cancer. *Rep. Pract. Oncol. Radiother.*, *15*(6), 176–180.
24. Martelli, S., & Chow, J. C. L. (2020). Dose enhancement for the flattening-filter-free and flattening-filter photon beams in nanoparticle-enhanced radiotherapy: A Monte Carlo phantom study. *Nanomaterials*, *10*, 637.
25. Cho, S. H. (2005). Estimation of tumour dose enhancement due to gold nanoparticles during typical radiation treatments: A preliminary Monte Carlo study. *Phys. Med. Biol.*, *50*, N163–N173.
26. Chow, J. C. L., & Jubran, S. (2023). Depth dose enhancement in orthovoltage nanoparticle-enhanced radiotherapy: A Monte Carlo phantom study. *Micromachines*, *14*, 1230.
27. McMahon, S. J., Hyland, W. B., Muir, M. F., Coulter, J. A., Jain, S., Butterworth, K. T., Schettino, G.,

Dickson, G. R., Hounsell, A. R., O'Sullivan, J. M., Prise, K. M., Hirst, D. G., & Currell, F. J. (2011). Nanodosimetric effects of gold nanoparticles in megavoltage radiation therapy. *Radiother. Oncol.*, *100*(3), 412–416.
28. Malam, Y., Loizidou, M., & Seifalian, A. M. (2009). Liposomes and nanoparticles: nanosized vehicles for drug delivery in cancer. *Trend Pharmacol. Sci.*, *30*(11), 592–599.
29. Barreto, J. A., O'Malley, W., Kubeil, M., Graham, B., Stephan, H., & Spiccia, L. (2011). Nanomaterials: applications in cancer imaging and therapy. *Adv. Mater.*, *23*(12), 18–40.
30. Carter, J. D., Cheng, N. N., Qu, Y., Suarez, G. D., & Guo, T. (2007). Nanoscale energy deposition by X-ray absorbing nanostructures. *J. Phys. Chem. B*, *111*, 11622–11625.
31. Liu, C. -J., Wang, C. -H., Chen, S. -T., Chen, H. -H., Leng, W. -H., Chien, C. -C., Wang, C. -L., Kempson, I. M., Hwu, Y., Lai, T. -C., Hsiao, M., Yang, C. -S., Chen, Y. -J., & Margaritondo, G. (2010). Enhancement of cell radiation sensitivity by pegylated gold nanoparticles. *Phys. Med. Biol.*, *55*, 931–945.
32. Zhao, P., Li, N., & Astruc, D. (2013). State of the art in gold nanoparticle synthesis. *Coord. Chem. Rev.*, *257*, 638–665.
33. Alkilany, A. M., Thompson, L. B., Boulos, S. P., Sisco, P. N., & Murphy, C. J. (2012). Gold nanorods: their potential for photothermal therapeutics and drug delivery, tempered by the complexity of their biological interactions. *Adv. Drug Deliv. Rev.*, *64*, 190–199.
34. Gray, T., Bassiri, N., David, S., Patel, D. Y., Stathakis, S., Kirby, N., & Mayer, K. M. (2021). A detailed experimental and Monte Carlo analysis of gold nanoparticle dose enhancement using 6 MV and 18 MV external beam energies in a macroscopic scale. *Appl. Radiat. Isot.*, *171*, 109638.
35. Khodaei, A., Moradi, F., Oresegum, A., Zubair, H. T., Bradley, D. A., Ibrahim, A. S., & Abdul Rashid, H. A. (2024). Evaluation of TOPAS MC tool performance in optical photon transport and radioluminescence-based dosimetry. *Biomed. Phys. Eng. Express*, *10*, 055034.
36. Emfietzoglou, D., & Nikjoo, H. (2005). The effect of model approximations on single-collision distributions of low-energy electrons in liquid water. *Radiat. Res.*, *163*(1), 98–111.
37. Incerti, S., Kyriakou, I., Bernal, M. A., Bordage, M. C., Francis, Z., Guatelli, S., Ivanchenko, V., Karamitros, M., Lampe, N., Lee, S. B., Meylan, S., Min, C. H., Shin, W. G., Nieminen, P., Sakata, D., Tang, N., Villagrasa, C., Tran, H. N., & Brown, J. M. C. (2018). Geant4-DNA example applications for track structure simulations in liquid water: A report from the Geant4-DNA Project. *Med. Phys.*, *45*(8), 722–739.
38. Moradi, F., Jalili, M., Rezaee Enrahim Saraee, Kh., Khandaker, M. U., & Bradley, D. A. (2022). Geant4 track structure simulation of electron beam interaction with a gold nanoparticle. *Radiat. Phys. Chem.*, *200*, 110278.
39. Plante, I., & Cucinotta, F. A. (2009). Cross sections for the interactions of 1 eV–100 MeV electrons in liquid water and application to Monte Carlo simulation of HZE radiation tracks. *New J. Phys.*, *11*, 63047.
40. Faddegon, B., Ramos-Méndez, J., Schuemann, J., McNamara, A., Shin, J., Perl, J., & Paganetti, H. (2020). The TOPAS tool for particle simulation, a Monte Carlo simulation tool for physics, biology and clinical research. *Phys. Med.*, *72*, 114–121.
41. International Commission on Radiation Units and Measurements. (1989). *Tissue substitutes in radiation units and measurement*. Bethesda, USA: ICRU. (ICRU Report No. 44).
42. Robar, J. L., Riccio, S. A., & Martin, M. A. (2002). Tumour dose enhancement using modified megavoltage photon beams and contrast media. *Phys. Med. Biol.*, *47*, 2433–2449.
43. Butterworth, K. T., McMahon, S. J., Currell, F. J., & Prise, K. M. (2012). Physical basis and biological mechanisms of gold nanoparticle radiosensitization. *Nanoscale*, *4*, 4830–4838.